A REAL-TIME SYNTHESIS ORIENTED TANPURA MODEL

Maarten van Walstijn, Jamie Bridges, and Sandor Mehes

Sonic Arts Research Centre
School of Electronics, Electrical Engineering, and Computer Science
Queen's University Belfast, UK
{m.vanwalstijn,jbridges05,smehes01}@qub.ac.uk

ABSTRACT

Physics-based synthesis of tanpura drones requires accurate simulation of stiff, lossy string vibrations while incorporating sustained contact with the bridge and a cotton thread. Several challenges arise from this when seeking efficient and stable algorithms for real-time sound synthesis. The approach proposed here to address these combines modal expansion of the string dynamics with strategic simplifications regarding the string-bridge and string-thread contact, resulting in an efficient and provably stable time-stepping scheme with exact modal parameters. Attention is given also to the physical characterisation of the system, including string damping behaviour, body radiation characteristics, and determination of appropriate contact parameters. Simulation results are presented exemplifying the key features of the model.

1. INTRODUCTION

Among mechanically-induced sound effects naturally afforded by musical instruments, the generation of overtones in tanpura drone playing is one of the more spectacular and intriguing examples. In Indian musical tradition, the phenomenon is known as *jvari* (meaning 'life-giving'), and arises from the impactive interaction of the vibrating string with a hard-surfaced bridge. The player fine-tunes the effect by carefully positioning a thin thread between the bridge and the string (see Fig. 1).

As a vibrational phenomenon, the jvari effect has attracted scientific interest for almost a century, starting with the musical acoustics poineering work by Raman [1]. Several ways of analysing and modelling the vibrations of the tanpura and other 'flat-bridge' instruments such as the sitar, veena, and biwa have been proposed since, with the aims ranging from theoretical understanding (usually relying on simplifying assumptions regarding the nature of the interaction [2, 3, 4]) to more practical discrete-time simulation [5, 6] including several synthesis oriented studies [7, 8]. The problem also naturally bears some resemblance to various other cases involving collisions, including string-fingerboard contact in the guitar [9, 10], violin [11], and bass guitar [12, 13, 14].

Despite these advances, efficient and realistic synthesis of the sound of flat-bridge string instruments appears to have remained a somewhat elusive goal. One of the original difficulties, namely that of potential instability when incorporating collision forces, has recently been addressed more widely within a finite-difference context, by construction of time-stepping schemes that respect the energy balance inherent to the underlying continuous-domain model [15, 16, 17, 18]. Tanpura models based on such energy methods can reproduce the jvari effect by simulating distributed string-bridge collisions [17, 19, 20]. However the algorithms that implement these tanpura models are not particularly suited to sound synthesis because of the high computational burden resulting from the reliance on iterative solvers and from the high sample rates needed to alleviate numerical dispersion.

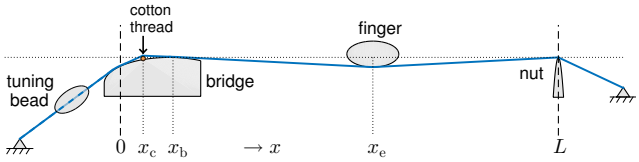

Figure 1: Schematic depiction of the tanpura string geometry (with altered proportions for clarity). The string termination points of the model are indicated with the vertical dashed lines.

This paper aims to formulate a leaner discrete-time tanpura string model requiring significantly reduced computational effort, but retaining much of the key sonic features of the instrument. Two aspects that distinguish this challenge somewhat from other cases of string-barrier interaction are (a) the sustained nature of the impactive interaction (with a high potential for audible high-frequency artefacts, including aliasing) and (b) the sensitivity of the jvari to some of the system parameters and to discretisation errors. The key features of the proposed model, presented in Section 2, can be summarised as follows:

- the spatially distributed string-bridge collision forces are suppressed to a single variable, which - in conjunction with neglecting contact damping and using a unity exponent in the contact law - allows updating the numerical system without the use of an iterative solver;
- the thread interaction, which effects a 'softer' string termination, is explicitly modelled as a local spring-damper connection;
- a modal expansion approach is utilised, which allows formulating a numerical model with exact modal frequencies and damping;
- discretisation is performed on a first-order partial derivative form of the modal differential equations, which facilitates the use of a two-point discrete gradient for discretisation of the bridge contact force;
- numerical stability is independent of the system parameters and the temporal step; the only numerical constraint is that the mode series is truncated at Nyquist in order to avoid mode aliasing.

For realistic synthesis of tanpura drones, one also needs to determine appropriate system parameters, including those related to string damping, bridge and thread contact, and sound radiation; this is discussed in Section 3. Exemplifying simulation results are then presented and discussed in Section 4, followed by concluding remarks and perspectives in Section 5.

2. TANPURA STRING MODEL

2.1. Model Equations

The transversal displacement $y(x,t)$ of the string depicted in Fig. 1, with the spatial domain defined as $x \in [0, L]$ and t denoting time, may be described by:

$$\rho A \frac{\partial^2 y}{\partial t^2} = T\frac{\partial^2 y}{\partial x^2} - EI\frac{\partial^4 y}{\partial x^4} - \gamma(\beta)\frac{\partial y}{\partial t} + \mathcal{F}_\mathrm{c}(x,t) + \mathcal{F}_\mathrm{b}(x,t) + \mathcal{F}_\mathrm{e}(x,t), \quad (1)$$

in which ρ, A, T, E, and I are mass density, cross-sectional area, tension, Young's modulus, and moment of inertia, respectively. Assuming simply supported ends, the boundary conditions are

$$y(x,t)\Big|_{x=0,L} = 0, \quad \frac{\partial^2 y}{\partial x^2}\Big|_{x=0,L} = 0. \quad (2)$$

Frequency-dependent string damping is incorporated by defining the parameter $\gamma(\beta)$ in (1) as:

$$\gamma(\beta) = 2\rho A\Big[\sigma_0 + \left(\sigma_1 + \sigma_3\beta^2\right)|\beta|\Big], \quad (3)$$

where β is the wave number and $\sigma_{0,1,3}$ are fit parameters. The interactions with the cotton thread, the bridge and a plucking finger are modelled using the force densities $\mathcal{F}_\mathrm{c}(x,t)$, $\mathcal{F}_\mathrm{b}(x,t)$ and $\mathcal{F}_\mathrm{e}(x,t)$, respectively. These are defined here in a simplified form by pre-determining their spatial distributions, hence modelling each as ($z = \mathrm{c}, \mathrm{b}, \mathrm{e}$):

$$\mathcal{F}_z(x,t) = \psi_z(x) F_z(t), \quad (4)$$

where $\psi_z(x)$ are spatial distribution functions of the form

$$\psi_z(x) = \begin{cases} \frac{\pi}{2w_z}\cos\left[\frac{\pi}{w_z}(x - x_z)\right] & : \quad x \in D_z \\ 0 & : \quad \text{otherwise} \end{cases} \quad (5)$$

in which $D_z = [x_z - \frac{1}{2}w_z, x_z - \frac{1}{2}w_z]$ denotes a spatial domain of width w_z and centre position x_z. Equation (5) is a good approximation to the force profile typically observed in the initial vibrations as computed with distrubuted contact models (see the left plot of Fig. 2). In addition this form provides a convenient way of exciting mainly the first mode of the string (by setting $x_\mathrm{e} = \frac{1}{2}L$, $w_\mathrm{e} = L$). The impactive contact with the bridge is modelled here using a lossless contact law with unity exponent and elasticity constant k_b:

$$F_\mathrm{b}(t) = k_\mathrm{b}\lfloor h_\mathrm{b} - y_\mathrm{b}(t)\rfloor, \quad (6)$$

in which $\lfloor y \rfloor$ denotes $u(y)\cdot y$, where $u(y)$ is the unit step function. Given that the string never detaches from the cotton thread, this interaction can be modelled as a simple spring-damper connection

$$F_\mathrm{c}(t) = k_\mathrm{c}\left[h_\mathrm{c} - y_\mathrm{c}(t)\right] - r_\mathrm{c}\frac{\partial y_\mathrm{c}}{\partial t}, \quad (7)$$

where r_c is a damping parameter. The term $y_z(t)$ ($z = \mathrm{b}, \mathrm{c}$) in equations (6) and (7) represents a spatially averaged value of the string displacement at x_z:

$$y_z(t) = \int_{x_z - w_z/2}^{x_z + w_z/2} \psi_\mathrm{z}(x)\, y(x,t)dx. \quad (8)$$

The contact potential energies are

$$V_\mathrm{c}(y_\mathrm{c}) = \frac{k_\mathrm{c}}{2}\left[h_\mathrm{c} - y_\mathrm{c}\right]^2, \quad V_\mathrm{b}(y_\mathrm{b}) = \frac{k_\mathrm{b}}{2}\lfloor h_\mathrm{b} - y_\mathrm{b}\rfloor^2, \quad (9)$$

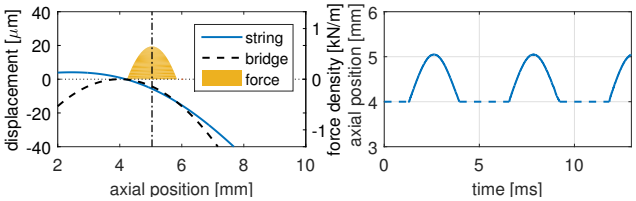

Figure 2: Left: string motion snapshot obtained with a model simulating distributed bridge contact [28]. The profile of the orange surface indicates force density, and the dash-dot line indicates the corresponding instantaneous central contact point. Right: Variation of the central contact point over the first 12ms. The flat dashed lines indicates periods of no contact.

where both height constants h_c and h_b are normally zero to ensure grazing contact at equilibrium. From the second equation it is straightforward to derive that

$$F_\mathrm{b}(t) = -\frac{\partial V_\mathrm{b}}{\partial y_\mathrm{b}}. \quad (10)$$

The forces exerted by the string at the left-end termination ('o') and the nut end ('n') are

$$F_\mathrm{o}(t) = T\frac{\partial y}{\partial x}\Big|_{x=0} - EI\frac{\partial^3 y}{\partial x^3}\Big|_{x=0}, \quad (11)$$

$$F_\mathrm{n}(t) = -T\frac{\partial y}{\partial x}\Big|_{x=L} + EI\frac{\partial^3 y}{\partial x^3}\Big|_{x=L}. \quad (12)$$

Since $F_\mathrm{o}(t)$ is generally much smaller than $F_\mathrm{c}(t)$ and $F_\mathrm{b}(t)$, the total force exerted by the string on the bridge can be calculated as

$$F_\mathrm{d}(t) = -F_\mathrm{c}(t) - F_\mathrm{b}(t). \quad (13)$$

Approximations to the emitted sound can be found by filtering $F_\mathrm{d}(t)$ and $F_\mathrm{n}(t)$, where the filters have transfer functions that approximate measured body radiation responses (see Section 3.3).

The plucking force is specified here in highly simplified form:

$$F_\mathrm{e}(t) = \begin{cases} a_\mathrm{e}\sin^2\left[(\pi/\tau_\mathrm{e})\, h_\mathrm{e}(t - t_\mathrm{e})\right] & : \quad t \in \mathcal{T}_\mathrm{e} \\ 0 & : \quad \text{otherwise} \end{cases}, \quad (14)$$

where $\mathcal{T}_\mathrm{e} = [t_\mathrm{e}, t_\mathrm{e} + \tau_\mathrm{e}]$ and with

$$h_\mathrm{e}(t) = \frac{1}{2}\left[t + \frac{\tau_\mathrm{e}\sinh(\beta_\mathrm{e} t/\tau_\mathrm{e})}{\sinh(\beta_\mathrm{e})}\right]. \quad (15)$$

As seen in Fig. 3, the parameter $\beta_\mathrm{e} > 0$ controls the attack and release slopes of the plucking function, which allows mimicking the gentle style in which tanpura strings are generally plucked. The other control parameters are the amplitude a_e and the overall pluck signal timespan τ_e. More sophisticated plucking models have been proposed (see, e.g. [9]) but may not be needed given that the characteristics of the tanpura sound are heavily dominated by the nonlinearity of the string-bridge interaction, with relatively little dependence on the intricacies of the finger-string interaction.

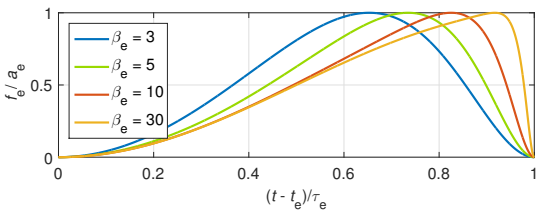

Figure 3: Normalised plucking force signal for four values of β_e.

2.2. Modal Expansion

The solution of (1) can be expressed as a superposition of the normal modes of the string (indexed with i):

$$y(x,t) = \sum_{i=1}^{M} v_i(x)\, \bar{y}_i(t), \tag{16}$$

where $\bar{y}_i(t)$ denotes the mode displacement and $v_i(x) = \sin(\beta_i x)$ is the corresponding mode shape (spatial eigenfunction) for the boundary conditions given in (2), with $\beta_i = i\pi/L$. After substitution of (16) into (1), then multiplying with $v_i(x)$ and applying a spatial integral over the length of the string, one obtains that the dynamics of each of the modes is governed by:

$$m\frac{\partial^2 \bar{y}_i}{\partial t^2} = -k_i \bar{y}_i(t) - r_i \frac{\partial \bar{y}_i}{\partial t} + \sum_{z=\mathrm{c,b,e}} \bar{F}_{\mathrm{z},i}(t), \tag{17}$$

in which $m = \frac{1}{2}\rho A L$ is the modal mass (which is the same for all modes), and where $k_i = \frac{1}{2}L\left(EI\beta_i^4 + T\beta_i^2\right)$ and $r_i = \frac{1}{2}L\gamma(\beta_i)$ are the elastic and damping constants of the mode, respectively. Within the constraint $r_i < 2\sqrt{k_i m}$, the modal frequencies are $\omega_i = \sqrt{k_i/m - \alpha_i^2}$, where (in accordance with (3))

$$\alpha_i = r_i/(2m) = \sigma_0 + \sigma_1\beta_i + \sigma_3\beta_i^3 \tag{18}$$

are the modal decay rates. The force terms in (17) are

$$\bar{F}_{z,i}(t) = \int_0^L v_i(x)\psi_z(x)F_z(t)dx = g_{z,i}F_z(t), \tag{19}$$

where[1]:

$$g_{z,i} = \frac{\pi^2 \sin(\beta_i x_z)\cos(\beta_i w_z/2)}{\pi^2 - \beta_i^2 w_z^2}. \tag{20}$$

In modal form, the spatially averaged string displacement at $x = x_z$ ($z = \mathrm{c, b}$) is

$$y_z(t) = \int_{x_z - w_z/2}^{x_z + w_z/2} \psi_z(x) \sum_{i=1}^{M} v_i(x)\bar{y}_i(t)dx = \sum_{i=1}^{M} g_{z,i}\bar{y}_i(t), \tag{21}$$

and the nut force can be expanded as

$$F_{\mathrm{n}}(t) = \sum_{i=1}^{M}\Big[-Tv_i'(L) + EIv_i'''(L)\Big]\bar{y}_i(t), \tag{22}$$

where $v_i'(x)$ and $v_i'''(x)$ denote the first and third spatial derivative of $v_i(x)$, respectively.

2.3. Discretisation in Time

We may re-formulate (17) in first-order form as follows:

$$\frac{\partial \bar{y}_i}{\partial t} = \frac{\bar{p}_i}{m}, \tag{23}$$

$$\frac{\partial \bar{p}_i}{\partial t} = -k_i\bar{y}_i - r_i\frac{\partial \bar{y}_i}{\partial t} + \sum_{z=\mathrm{c,b,e}} g_{z,i}F_z(t), \tag{24}$$

in which $\bar{p}_i$ represents the modal momentum. Gridding time by denoting $y^n \equiv y(n\Delta t)$, where $\Delta t = {f_\mathrm{s}}^{-1}$ is the temporal step, we introduce the difference and sum operators

$$\delta y^n = y^{n+\frac{1}{2}} - y^{n-\frac{1}{2}} \approx \Delta t\, \frac{\partial y}{\partial t}\Big|_{t=n\Delta t}, \tag{25}$$

$$\mu y^n = y^{n+\frac{1}{2}} + y^{n-\frac{1}{2}} \approx 2\, y\Big|_{t=n\Delta t}. \tag{26}$$

[1] Note that care has to be taken in evaluating (20) for $\beta_i = w_z/\pi$, using $\lim_{\beta_i \to w_z/\pi} g_{z,i} = \frac{\pi}{4}\sin(\beta_i x_z)$.

The mid-point-in-time discretisation of equations (23) and (24) can then be written as

$$\frac{\delta \bar{y}_i^{n+\frac{1}{2}}}{\Delta t} = \frac{\mu \bar{p}_i^{n+\frac{1}{2}}}{2m}, \tag{27}$$

$$\frac{\delta \bar{p}_i^{n+\frac{1}{2}}}{\Delta t} = -k_i\frac{\mu \bar{y}_i^{n+\frac{1}{2}}}{2} - r_i\frac{\delta \bar{y}_i^{n+\frac{1}{2}}}{\Delta t} + \sum_{z=\mathrm{c,b,e}} g_{z,i}F_z^{n+\frac{1}{2}}, \tag{28}$$

which is equivalent to applying the trapezoidal rule. The external force is calculated as $\frac{1}{2}\mu F_\mathrm{e}^{n+\frac{1}{2}}$, and the cotton thread force is obtained by discretising (7):

$$F_\mathrm{c}^{n+\frac{1}{2}} = k_\mathrm{c}\left(h_\mathrm{c} - \tfrac{1}{2}\mu y_\mathrm{c}^{n+\frac{1}{2}}\right) - r_\mathrm{c}\frac{\delta y_\mathrm{c}^{n+\frac{1}{2}}}{\Delta t}. \tag{29}$$

Special care has to be taken regarding stability in discretising the bridge contact force, due to its non-analytic form [15, 16]. A suitable numerical term is obtained by discretising (10), which yields the two-point discrete gradient:

$$F_\mathrm{b}^{n+\frac{1}{2}} = -\frac{\delta V_\mathrm{b}^{n+\frac{1}{2}}}{\delta y_\mathrm{b}^{n+\frac{1}{2}}} = -\frac{V_\mathrm{b}(y_\mathrm{b}^{n+1}) - V_\mathrm{b}(y_\mathrm{b}^n)}{y_\mathrm{b}^{n+1} - y_\mathrm{b}^n}. \tag{30}$$

Using the scaled momentum value $\bar{q}_i^n = (\Delta t/(2m))\bar{p}_i^n$, the system equations (27,28) can be written more conveniently as

$$\delta \bar{y}_i^{n+\frac{1}{2}} = \mu \bar{q}_i^{n+\frac{1}{2}}, \tag{31}$$

$$\delta \bar{q}_i^{n+\frac{1}{2}} = -a_i\mu \bar{y}_i^{n+\frac{1}{2}} - b_i\delta \bar{y}_i^{n+\frac{1}{2}} + \xi \sum_{z=\mathrm{c,b,e}} g_{z,i}F_z^{n+\frac{1}{2}}, \tag{32}$$

where $\xi = \Delta t^2/(2m)$, $a_i = \frac{1}{4}k_i\Delta t^2\, m^{-1}$, and $b_i = \frac{1}{2}r_i\Delta t m^{-1}$. Once the force terms $F_z^{n+\frac{1}{2}}$ are known, the dynamics of each mode can be simulated by solving for $\bar{y}_i^{n+1}$ and $\bar{q}_i^{n+1}$ at each time step. However, unless a very small temporal step is used, this procedure would lead to severe numerical dispersion. Therefore the coefficients in (31,32) are replaced by the values (a_i^*, b_i^*) below, which ensures that the modes have exact modal frequencies and damping:

$$a_i^* = \frac{1 - 2R_i\Omega_i + R_i^2}{1 + 2R_i\Omega_i + R_i^2}, \quad b_i^* = \frac{2\left(1 - R_i^2\right)}{1 + 2R_i\Omega_i + R_i^2}, \tag{33}$$

where $R_i = \exp(-\alpha_i\Delta t)$ and $\Omega_i = \cos(\omega_i\Delta t)$. This is readily verified by testing the (31,32) without the force terms for the ansatz

$$\bar{y}_i^n = \exp(s_\mathrm{d} n\Delta t), \quad \bar{q}_i^n = C\exp(s_\mathrm{d} n\Delta t), \tag{34}$$

where $s_\mathrm{d} = \mathrm{j}\omega_\mathrm{d} - \alpha_\mathrm{d}$ is the complex resonance frequency of the discretised mode, with $\mathrm{j} = \sqrt{-1}$, and C is a complex constant. This leads to a characteristic equation in $z_\mathrm{d} = \exp(s_\mathrm{d}\Delta t)$:

$$z_\mathrm{d}^2 - 2\left(\frac{1 - a_i}{1 + a_i + b_i}\right)z_\mathrm{d} + \left(\frac{1 + a_i - b_i}{1 + a_i + b_i}\right) = 0. \tag{35}$$

After substituting (33) this becomes

$$z_\mathrm{d}^2 - 2R_i\cos(\omega_i\Delta t)z_\mathrm{d} + R_i^2 = 0, \tag{36}$$

which has the solution $z_\mathrm{d} = R_i\exp(\omega_i\Delta)$, from which it follows that $s_\mathrm{d} = \mathrm{j}\omega_i - \alpha_i$, i.e. the discrete system has exact modal frequency and damping. The above coefficient replacement can be thought of in terms of the following adapted elasticity and damping values:

$$k_i \to k_i^* = \frac{4ma_i^*}{\Delta t^2}, \quad r_i \to r_i^* = \frac{2mb_i^*}{\Delta t}. \tag{37}$$

An accompanying restriction - necessary to avoid aliased modes - is that none of mode frequencies exceeds the Nyquist frequency, i.e. $\omega_i < \pi/\Delta t$, which defines the largest possible truncation of the modal series expansion in (16). A seemingly simpler way to avoid numerical dispersion is to discretize (17) using the impulse invariant transform and defining (30) in three-point form. However the resulting model would not be provably stable due to mode dependency of the modal force coefficients, which precludes defining an energy balance with non-negative energy.

2.4. A Vector-Matrix Update Form

If we stack the variables in column vector form, for M modes we may write the system equations as

$$\delta\bar{\mathbf{y}}^{n+\frac{1}{2}} = \mu\bar{\mathbf{q}}^{n+\frac{1}{2}}, \tag{38}$$

$$\delta\bar{\mathbf{q}}^{n+\frac{1}{2}} = -\mathbf{A}\mu\bar{\mathbf{y}}^{n+\frac{1}{2}} - \mathbf{B}\delta\bar{\mathbf{y}}^{n+\frac{1}{2}} + \xi \sum_{z=\mathrm{c,b,e}} \mathbf{g}_z F_z^{n+\frac{1}{2}}, \tag{39}$$

where $\mathbf{A}$ and $\mathbf{B}$ are diagonal matrices with diagonal entries $A_{ii} = a_i^*$ and $B_{ii} = b_i^*$, and where column vectors $\mathbf{g}_z$ hold the values defined with (20). A convenient vector update is then found by using (38) to define $\bar{\mathbf{s}} = \delta\bar{\mathbf{y}}^{n+\frac{1}{2}} = \mu\bar{\mathbf{q}}^{n+\frac{1}{2}}$, and substituting

$$\bar{\mathbf{y}}^{n+1} = \bar{\mathbf{s}} + \bar{\mathbf{y}}^n, \quad \bar{\mathbf{q}}^{n+1} = \bar{\mathbf{s}} - \bar{\mathbf{q}}^n, \tag{40}$$

in (39), which allows solving for $\bar{\mathbf{s}}$ with

$$\bar{\mathbf{s}} = \bar{\mathbf{u}} + \mathbf{e}_\mathrm{b} F_\mathrm{b}^{n+\frac{1}{2}} + \mathbf{e}_\mathrm{c} F_\mathrm{c}^{n+\frac{1}{2}}, \tag{41}$$

where $\mathbf{e}_\mathrm{b} = \xi\mathbf{J}^{-1}\mathbf{g}_\mathrm{b}$ and $\mathbf{e}_\mathrm{c} = \xi\mathbf{J}^{-1}\mathbf{g}_\mathrm{c}$, with $\mathbf{J} = \mathbf{I} + \mathbf{A} + \mathbf{B}$, and where

$$\bar{\mathbf{u}} = \mathbf{J}^{-1}\Big[2\left(\bar{\mathbf{q}}^n - \mathbf{A}\bar{\mathbf{y}}^n\right) + \xi\mathbf{g}_\mathrm{e} F_\mathrm{e}^{n+\frac{1}{2}}\Big]. \tag{42}$$

Hence once the contact forces $F_\mathrm{b}^{n+\frac{1}{2}}$ and $F_\mathrm{c}^{n+\frac{1}{2}}$ are known, eq. (41) immediately yields the step $\bar{\mathbf{s}}$, after which both $\bar{\mathbf{y}}^{n+1}$ and $\bar{\mathbf{q}}^{n+1}$ can be updated using (40). A further update comprises evaluating the nut force $F_\mathrm{n}^{n+\frac{1}{2}}$ with the vector form of (22). Note that since the matrices $\mathbf{J}$ and $\mathbf{A}$ are diagonal, the matrix operations in (42) can be implemented very efficiently via componentwise multiplication/division.

2.5. Solving for the Contact Forces

In order to solve for the forces $F_\mathrm{b}^{n+\frac{1}{2}}$ and $F_\mathrm{c}^{n+\frac{1}{2}}$, (41) is pre-multiplied with $\mathbf{g}_\mathrm{b}^\mathsf{T}$, which (also using $s_\mathrm{b} = y_\mathrm{b}^{n+1} - y_\mathrm{b}^n$) yields the scalar equation

$$s_\mathrm{b} = u_\mathrm{b} + \theta_\mathrm{bb} F_\mathrm{b}^{n+\frac{1}{2}} + \theta_\mathrm{bc} F_\mathrm{c}^{n+\frac{1}{2}}, \tag{43}$$

where $u_\mathrm{b} = \mathbf{g}_\mathrm{b}^\mathsf{T}\bar{\mathbf{u}}$, $\theta_\mathrm{bb} = \mathbf{g}_\mathrm{b}^\mathsf{T}\mathbf{e}_\mathrm{b}$ and $\theta_\mathrm{bc} = \mathbf{g}_\mathrm{b}^\mathsf{T}\mathbf{e}_\mathrm{c}$. Similarly, one can pre-multiply (41) with $\mathbf{g}_\mathrm{c}^\mathsf{T}$, giving

$$s_\mathrm{c} = u_\mathrm{c} + \theta_\mathrm{bc} F_\mathrm{b}^{n+\frac{1}{2}} + \theta_\mathrm{cc} F_\mathrm{c}^{n+\frac{1}{2}}, \tag{44}$$

with $u_\mathrm{c} = \mathbf{g}_\mathrm{c}^\mathsf{T}\bar{\mathbf{u}}$ and $\theta_\mathrm{cc} = \mathbf{g}_\mathrm{c}^\mathsf{T}\mathbf{e}_\mathrm{c}$. Setting $\phi_\mathrm{c} = k_\mathrm{c}/2 + r_\mathrm{c}/\Delta t$, the numerical thread force in equation (29) can be written in terms of s_c as

$$F_\mathrm{c}^{n+\frac{1}{2}} = k_\mathrm{c}\left(h_\mathrm{c} - y_\mathrm{c}^n\right) - \phi_\mathrm{c} s_\mathrm{c}. \tag{45}$$

Combining with (44) to eliminate s_c then gives

$$F_\mathrm{c}^{n+\frac{1}{2}} = v_\mathrm{c} - \beta_\mathrm{c} F_\mathrm{b}^{n+\frac{1}{2}}, \tag{46}$$

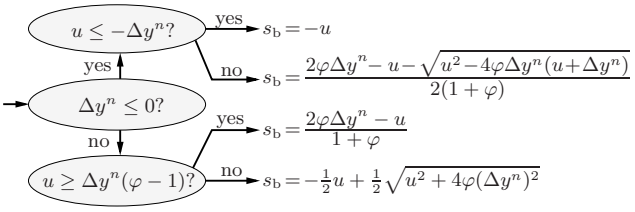

Figure 4: Analytic solution of equation (48), where $\varphi = \theta k_\mathrm{b}/2$ and $\Delta y^n = h_\mathrm{b} - y_\mathrm{b}^n$.

where

$$v_\mathrm{c} = \frac{k_\mathrm{c}\left(h_\mathrm{c} - y_\mathrm{c}^n\right) - \phi_\mathrm{c} u_\mathrm{c}}{1 + \phi_\mathrm{c}\theta_\mathrm{cc}}, \quad \beta_\mathrm{c} = \frac{\phi_\mathrm{c}\theta_\mathrm{bc}}{1 + \phi_\mathrm{c}\theta_\mathrm{cc}}. \tag{47}$$

Now substituting this into (43) and evaluating the bridge force term with (30) one obtains the nonlinear scalar equation

$$s_\mathrm{b} + u + \theta\frac{V_\mathrm{b}(s_\mathrm{b} + y_\mathrm{b}^n) - V_\mathrm{b}(y_\mathrm{b}^n)}{s_\mathrm{b}} = 0, \tag{48}$$

where $\theta = \theta_\mathrm{bb} - \beta_\mathrm{c}\theta_\mathrm{bc}$ and $u = -u_\mathrm{b} - \theta_\mathrm{bc} v_\mathrm{c}$. This equation is analytically solvable according to four distinct cases [18] as shown in Fig. 4. Once s_b is known the bridge force can be calculated accordingly and the thread force is updated with (46).

2.6. Numerical Energy Balance and Stability

The energy of the numerical model can be calculated for any time instant n by summing up the mode energies and adding the potentials of the bridge and thread interaction:

$$\begin{aligned} H^n &= \sum_{i=1}^{M}\left[\frac{1}{2m}(\bar{p}_i^n)^2 + \frac{k_i^*}{2}(\bar{y}_i^n)^2\right] + V_\mathrm{c}(y_\mathrm{c}^n) + V_\mathrm{b}(y_\mathrm{b}^n) \\ &= \frac{(\bar{\mathbf{q}}^n)^\mathsf{T}\bar{\mathbf{q}}^n + (\bar{\mathbf{y}}^n)^\mathsf{T}\mathbf{A}\bar{\mathbf{y}}^n}{\xi} + \frac{k_\mathrm{c}}{2}\left[h_\mathrm{c} - y_\mathrm{c}^n\right]^2 + \frac{k_\mathrm{b}}{2}\lfloor h_\mathrm{b} - y_\mathrm{b}^n\rfloor^2. \end{aligned} \tag{49}$$

Multiplying the left-hand side of (39) with $(\mu\bar{\mathbf{q}}^{n+\frac{1}{2}})^\mathsf{T}$ and the right-hand side with $(\delta\bar{\mathbf{y}}^{n+\frac{1}{2}})^\mathsf{T}$ yields, after a few further algebraic manipulations, the energy balance

$$\frac{\delta H^{n+\frac{1}{2}}}{\Delta t} = P^{n+\frac{1}{2}} - Q^{n+\frac{1}{2}}, \tag{50}$$

where

$$P^{n+\frac{1}{2}} = \tfrac{1}{2}\Delta t^{-1}\mathbf{g}_\mathrm{e}^\mathsf{T}\delta\bar{\mathbf{y}}^{n+\frac{1}{2}}\mu F_\mathrm{e}^{n+\frac{1}{2}} \tag{51}$$

is the input power and

$$Q^{n+\frac{1}{2}} = \frac{(\delta\bar{\mathbf{y}}^{n+\frac{1}{2}})^\mathsf{T}\mathbf{B}\delta\bar{\mathbf{y}}^{n+\frac{1}{2}}}{\xi\Delta t} + \left(\frac{r_\mathrm{c}}{\Delta t^2}\right)\left(\delta y_\mathrm{c}^{n+\frac{1}{2}}\right)^2 \tag{52}$$

is the dissipated power. From inspecting (33), it follows that the diagonal matrices $\mathbf{A}$ and $\mathbf{B}$ can only contain real-valued positive elements and are thus positive definite. This implies unconditional numerical stability, as both H^n and $Q^{n+\frac{1}{2}}$ are consequently guaranteed to be non-negative (i.e. the total energy can increase only through external force excitation). It is worthwhile pointing out that the energy balance in (50) relies not only on the use of the discrete gradient in (30), but also on the fact that equations (4) and (8) utilise the same spatial distribution function, which ensures that the vector terms $\mathbf{g}_\mathrm{b}$ are eliminated in the calculation process.

3. PHYSICAL CHARACTERISATION

3.1. String Parameters

The string parameters L, A, E and ρ are readily available for a given string, and the tension T can be set accordingly such that the correct fundamental frequency results. The moment of inertia is calculated directly from the string radius r as $I = \frac{1}{4}\pi r^4$. The damping coeffcients $\sigma_{0,1,3}$ in (18) can be estimated from a plucked string signal measured with a freely vibrating string (i.e. no bridge contact), for example as in [21]. Given the importance of the role of string damping in the jvari effect, it is worthwhile noting that these coefficients can be expressed directly in terms of the physically motivated fit parameters used by Woodhouse in eq. (8) of [21] for characterising guitar strings:

$$\sigma_0 \approx \tfrac{1}{2}\eta_A, \quad \sigma_1 \approx \tfrac{1}{2}c\,\eta_F, \quad \sigma_3 \approx \tfrac{1}{2}c\,\lambda\,\eta_B, \tag{53}$$

with $c = \sqrt{T/(\rho A)}$ and $\lambda = EI/T$, and where η_A, η_F, and η_B represent "air", "friction", and "bending" damping, respectively. Woodhouse's modal decay rate form, which was adapted from [22], generally allows an excellent low-parameter fit to measured string data over a wide frequency range [22, 21]. For this reason equation (18) is preferred here over the even-order form $\alpha_i = \sum_j \sigma_j \beta_i^{2j}$ often used in sound synthesis.

Table 1: Physical parameter values used for a C_3 string.

string parameters			contact parameters		
L	1.0	[m]	x_b	10×10^{-3}	[m]
ρA	4.83×10^{-4}	[kg/m]	w_b	2.0×10^{-3}	[m]
T	33.1	[N]	k_b	4.39×10^{8}	[N/m]
EI	6.03×10^{-5}	[Nm^2]	x_c	[4.0 - 8.0]$\times10^{-3}$	[m]
σ_0	0.6	[s^{-1}]	w_c	1.2×10^{-3}	[m]
σ_1	6.5×10^{-3}	[m/s]	k_c	1.2×10^{5}	[N/m]
σ_3	5.0×10^{-6}	[m^3/s]	r_c	1.2	[kg/s]

3.2. Contact Parameters

The rationale for using a contact law with unity exponent is based on an analogy to contact between two cylinders with parallel axes. From Hertzian contact theory, the force F is proportional to the depth of indentation d for this case [23]:

$$F = \frac{\pi}{4} E^* l\, d, \tag{54}$$

where l is the contact length, with the contact modulus given as

$$E^* = \left(\frac{1-\nu_1^2}{2E_1} + \frac{1-\nu_2^2}{2E_2} \right)^{-1} \tag{55}$$

for materials with Young's moduli E_1, E_2 and Poisson's ratios ν_1, ν_2. This law is independent of the radii of the two cylinders and thus is applicable also to contact between a cylindrical string and a nearly flat surface. By loosely equating d and $\Delta y = h_\mathrm{b} - y_\mathrm{b}$ an estimate of the elastic constant in (6) is found as $k_\mathrm{b} = \frac{1}{4}\pi E^* w_\mathrm{b}$, with E^* evaluated using the values for steel (or bronze when applicable) and ivory in eq. (55). The cotton thread contact parameters are not as easily determined and are empirically set here as $k_\mathrm{c} = w_\mathrm{c} \cdot 10^8$ N/m and $r_\mathrm{c} = k_\mathrm{c} \cdot 10^{-6}$ N/m. The parameters used for a one metre long male tanpura string (steel, radius = 0.14mm) when tuned to the note C_3 ($f_1 = 130.81$Hz) are listed in Table 1.

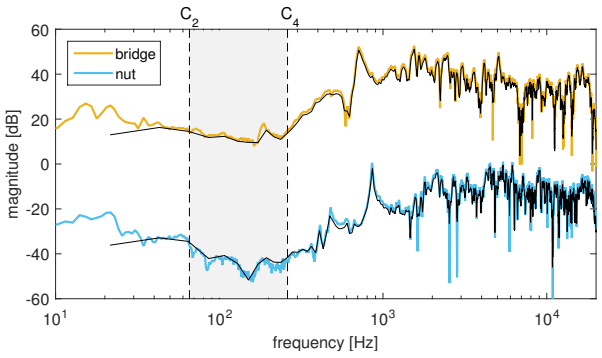

Figure 5: Tanpura body magnitude response measured with an impact hammer applied at the bridge (top) and the nut (bottom), and with a microphone positioned at 80cm from the instrument. For clarity, the responses have been offset by 50dB. The grey shaded area indicates the range in which the fundamental frequency of a tanpura string would normally fall.

3.3. Body Radiation Filters

Fig. 5 shows the body magnitude responses of a tanpura as obtained with impact hammer experiments. The fundamental frequency of a tanpura string will generally fall in the range between that of a C_2 string ($f_1 = 65.4$Hz) and a C_4 string ($f_1 = 198$Hz). As the plot shows, the body radiates less powerfully in this frequency range, to a first approximation acting as a high-pass filter. The black thin solid lines in Fig. 5 indicate the responses of 2048-tap FIR filters obtained by truncating the measured body impulse responses. Significantly more efficient body filters models can be achieved in IIR form (see, e.g. [24]).

4. SIMULATION RESULTS

4.1. Simulation of a C_3 String

Fig. 6 shows a small selection of string profile snapshots obtained with the simulation of a C_3 string, using the parameters listed in Table 1, with $x_\mathrm{c} = 5$mm. To exemplify the role of the bridge and the thread, the string was excited using $a_\mathrm{e} = -0.4$N, $\tau_\mathrm{e} = 50$ms, $\beta_\mathrm{e} = 30$, $x_\mathrm{e} = L/2$ and $w_\mathrm{e} = L$, effectively initialising the string approximately to the first mode shape. As seen in Fig. 6(a) the string motion becomes progressively Helmholz-like, as also found in earlier studies [22, 19]. The zoomed view in Fig. 6(b) shows that a small level of string motion is allowed at the thread position. The bridge on the other hand is far less compressive, approximating a one-sided constraint. The role of the cotton thread connection can be summarised as follows: the thread damping provides additional attenuation of the high-frequency standing waves along the string length between the left termination and the bridge, which in combination with the lower elasticity constant effects a 'soft' termination (somewhat similar to a violin string stopped by a finger rather than the nut). This avoids the harsher sound that would result with a (near) rigid termination.

Fig. 7 shows how the displacement at the bridge evolves over time. The string-bridge compression is extremely small (less than 3×10^{-8}m over the whole duration). The plots demonstrate the emergence of a high-frequency wavepacket in the waveforms. Due to string stiffness this precursive wave arrives back at the bridge before the lower frequencies, thus escaping the periodic closing of

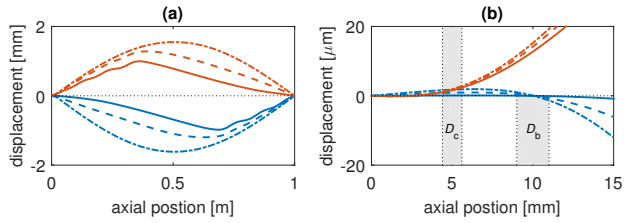

Figure 6: Snapshots of the profile of a C_3 string excited using the parameters $x_e = L/2$, $w_e = L$. The sampling frequency is 44.1kHz. Left: full string profile. Right: zoomed view of the thread/bridge region; the grey shaded rectangles indicate the force-active regions of the thread (D_c) and the bridge (D_b). For both plots, the time instants are t = 49.0ms (dash-dot blue), t = 52.6ms (dash-dot red), t = 208.4ms (dashed blue), t = 212.0ms (dashed red), t = 412.7ms (solid blue), t = 416.3ms (solid red).

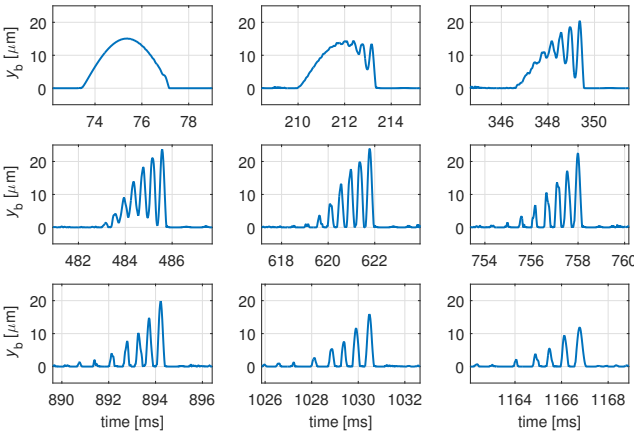

Figure 7: Evolution of the displacement (y_b) at the bridge.

the gap between the string and the bridge [3]. Running the simulation with $EI = 0$ confirms that the precursor, which is the principal oscillatory manifestation of the jvari effect, disappears in the absence of string stiffness. As can be gleaned from the plots, the spectral centroid of the precursor gradually diminishes over time, which is due to the string damping being frequency-dependent. The rate at which the centroid descends also depends on the distance between the bridge and the thread [3]; this is one of the sonic features that tanpura players control when, in preparation of a performance, they adjust the thread position in search of a desired jvari.

Fig. 8(a) shows the global evolution of the driving forces F_d and F_n. Comparison with the corresponding pressure signals p_d and p_n shown in Fig. 8(b) highlights the difference in terms of the initial attack transient, which is almost completely absent from the radiation signals; this is because they contain much less of the low-frequency excitation components and are dominated by the frequencies that make up the precursor. The aural impression is therefore that the sound grows in amplitude over the initial 500ms, which is contrary to our normal experience of plucked strings. These results suggest that the high-pass nature of the body responses (explained earlier in Section 3.3) is a key ingredient in producing this effect, which is further enhanced by the frequency-dependent sensitivity of human hearing [3].

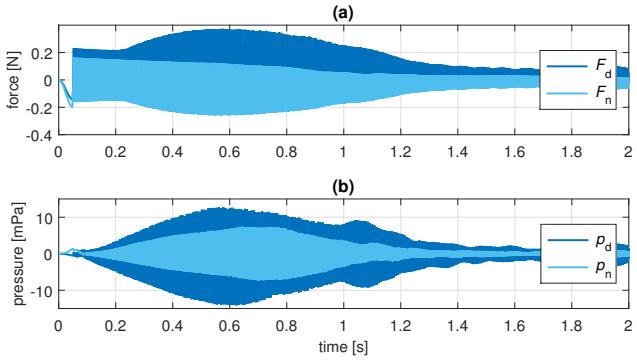

Figure 8: Waveforms of the bridge and nut driving force signals (a) and the corresponding radiation pressure signals (b).

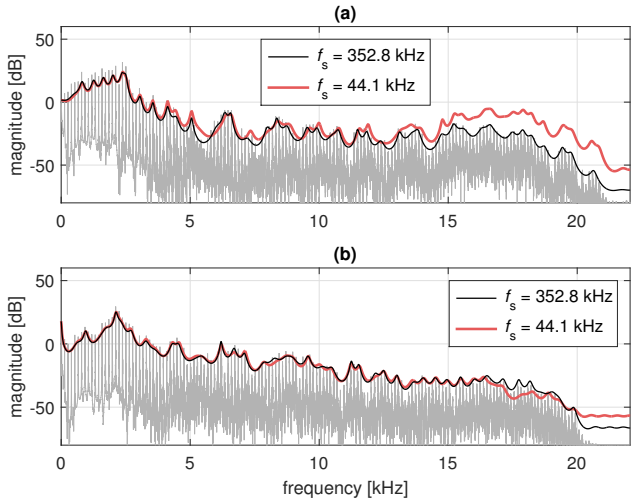

Figure 9: Spectral envelopes of the bridge radiation pressure signal (a) and the nut radiation signal (b), for different sampling frequencies. In each plot, the magnitude spectrum obtained with eight times oversampling (f_s =352.8kHz) is plotted in light grey.

4.2. Convergence

In a sound synthesis context, it is natural to use a standard audio rate. However mainly due to the nonlinear phenomena, the model will not give exactly the same result as for higher sampling frequencies, even when the number of modes is kept the same. Fig. 9 shows the magnitude spectra (light grey line) of the radiation signals p_d and p_n, as obtained with for a C_3 string using eight times oversampling. In each of the plots the thin black line represents the corresponding spectral envelope while the thicker, red line indicates the envelope of the spectrum obtained using $f_s = 44.1$kHz. For both sampling frequencies, the number of modes was set to 133, which corresponds to truncating the mode series at 20kHz. The plots show that while there is little difference between the nut radiation signals, the 44.1kHz model bridge signal is artificially strong in amplitude at high frequencies ($f > 15$kHz). Perceptually, the discrepancy is very small but nevertheless noticeable. Informal listening experiments indicated that oversampling by a factor two (i.e. using $f_s = 88.2$kHz) is sufficient to reduce any differences to almost unnoticeable levels.

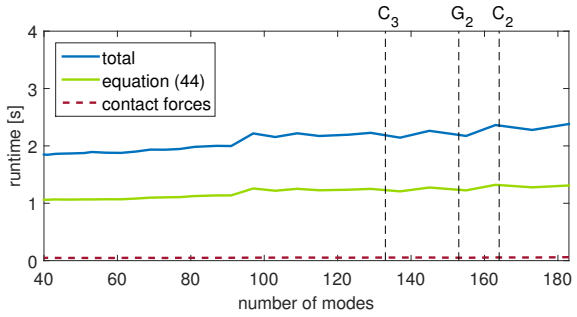

Figure 10: `Matlab` computation times for one second of simulated sound when using a 44.1kHz sampling frequency. The results were obtained using a machine with an i7 CPU 2.93GHz processor and 4GB RAM.

4.3. Algorithmic Efficiency

The `Matlab` runtime for one second of simulation (see Fig. 10) is only mildly dependent on the number of modes included and does not exceed 2.5 seconds for any practical string (compared to 2 minutes with the model in [19], which requires four times oversampling in order to alleviate numerical dispersion). A significant speed-up is achievable with an optimised C implementation, bringing the proposed model in range for real-time application on standard processors. Note that the filtering of the nut and bridge driving signals is not included in the computational operations that are time-measured. As is evident from the plot, more than half of the computational effort comprises updating equation (42), while solving for the contact forces takes up an almost negligible fraction.

4.4. Drone Synthesis

In order to get a first glimpse of what a virtual-acoustic tanpura would sound like, four separate string models were tuned to produce a *panchamam* raga pattern of G_2-C_3-C_3-C_2. The total bridge and nut driving forces are now

$$\hat{F}_\mathrm{d} = -\sum_{j=1}^{4} \left(F_{\mathrm{c},j} + F_{\mathrm{b},j}\right), \quad \hat{F}_\mathrm{n} = \sum_{j=1}^{4} F_{\mathrm{n},j}, \qquad (56)$$

where subscript j indexes the strings. These are filtered as before with the body radiation filters, with the filter outputs p_d and p_n assigned to the left and right channel of an audio signal; a sound example can be found on the accompanying webpage[2] alongside further supporting material. Fig. 11 shows the spectrogram of the total bridge force $\hat{F}_\mathrm{d}$ for a single drone cycle. The plot illustrates the migration of energy from the lower partials to higher frequency components. The precursors are manifested in the time-frequency representation as formants with descending centre frequencies. Also noticeable is that the precursors generated with the C_3 and C_2 strings together construct a joint, seamless jvari pattern, which adds to the sense of continuity of the drone [3].

5. CONCLUDING REMARKS AND PERSPECTIVES

The proposed model permits simulation of tanpura drones with significantly increased efficiency compared to previous models,

[2] `www.socasites.qub.ac.uk/mvanwalstijn/dafx16a/`

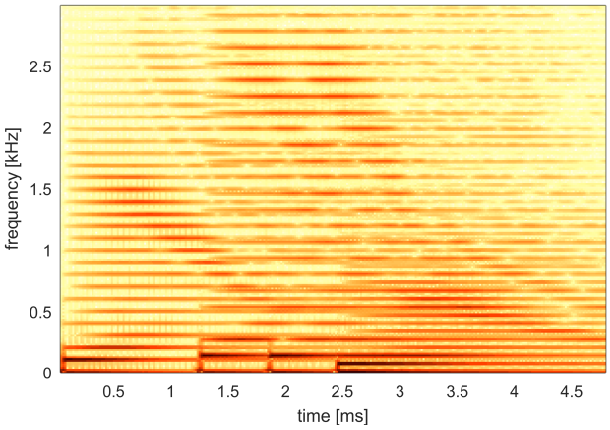

Figure 11: Spectrogram of a four-string tanpura bridge driving force signal. The strings were excited at $t_e = 0$, 1.2, 1.8, and 2.4s.

as such opening up possibilities for real-time implementation on standard processors. The modal approach taken results in spectral accuracy of the string resonance behaviour, and also facilitates efficient implementation due to the diagonality the system matrices.

Modal expansion is, of course, not a new concept in sound synthesis, originating some decades ago as *modal synthesis* [25]. It also underpins the more formalised *functional transformation method* [26, 13] and other modular approaches [27]. What is different in the approach presented here is that collision forces are incorporated in a provably stable manner, which is of particular importance in a real-time sound synthesis context.

The model could also be formulated in finite difference form, for example using a parametric implicit three-point scheme for the string [18] which can be tuned to closely approximate spectral accuracy. However for the relatively simple model proposed here this approach holds no efficiency advantages, since matrices would be sparse rather than diagonal. In addition, the three-point form of (30) is a less accurate approximation of the bridge contact force.

Among several possible model extensions, either in modal or finite difference form, probably the most important ones are (a) the simulation of sympathetic vibrations by also modelling the string-body coupling and (b) the re-introduction of distributed bridge collisions [28]. Because the latter effects a periodic modulation of the central contact point between the string and the bridge (see Fig. 2(b)), it would be sensible to consider this in conjunction with tension modulation, which is potentially relevant given that tanpura strings are loosely strung. The literature already contains various techniques for incorporating tension modulation into modal schemes [26, 29, 27] and finite difference formulations [30], but the proposed two-point scheme requires a re-formulation. Such extensions would pave the way for a rigorous evaluatory comparison between the proposed model, more complete models, and measurement data. However they will also increase the complexity and computational load of the model, meaning real-time synthesis may be viable only via hardware acceleration, such as graphical processing units [31] or field programmable arrays [32].

Besides model refinements and extensions, the most pertinent advance may be the implementation of a real-time virtual-acoustic tanpura that affords real-time control options. This would allow fine-tuning of the jvari effect by ear through on-line adjustment of the parameters of the string, thread, and bridge, much in the same way as real-world tanpura players set up their instrument.

6. REFERENCES

[1] C. Raman, "On some indian stringed instruments," in *Proc. of the Indian Assoc. for the Cultivation of Science*, 1921, vol. 7, pp. 29–33.

[2] R. Burridge, J. Kappraff, and C. Morshedi, "The sitar string, a vibrating string with a one-sided inelastic constraint," *SIAM J. Appl. Mathematics*, vol. 42, no. 6, pp. 1231–1251, 1982.

[3] C. Valette, C. Cuesta, C. Besnainou, and M. Castellengo, "The tanpura bridge as a precursive wave generator," *Acustica*, vol. 74, pp. 201–208, 1991.

[4] C. Vyasarayani, S. Birkett, and J. McPhee, "Modeling the dynamics of a vibrating string with a finite distributed unilateral constraint: Application to the sitar," *J. Acoust. Soc. Am.*, vol. 125, no. 6, pp. 3673–3682, 2009.

[5] T. Taguti, "Dynamics of simple string subject to unilateral constraint: A model analysis of sawari mechanism," *Acoust. Sci. Technol.*, vol. 29, no. 3, pp. 203–214, 2008.

[6] D. Kartofelev, A. Stulov, H. Lehtonen, and V. Välimäki, "Modeling a vibrating string terminated against a bridge with arbitrary geometry," in *Stockholm Musical Acoustics Conf.*, 2013.

[7] A. Krishnaswamy and J. Smith, "Methods for simulating string collisions with rigid spatial obstacles," in *Proc. IEEE WASPAA*, New York, 2003.

[8] S. Siddiq, "A Physical Model of the Nonlinear Sitar String," *Archives of Acoustics*, vol. 37, no. 1, Jan. 2012.

[9] G. Evangelista and F. Eckerholm, "Player-instrument interaction models for digital waveguide synthesis of guitar: Touch and collisions," *IEEE Trans. Audio, Speech and Lang. Proc.*, vol. 18, no. 4, pp. 822–832, 2010.

[10] S. Bilbao and A. Torin, "Numerical modeling and sound synthesis for articulated string/fretboard interactions," *J. Audio Eng. Soc.*, vol. 63, pp. 336–347, 2015.

[11] C. Desvages and S. Bilbao, "Two-polarisation finite difference model of bowed strings with nonlinear contact and friction forces," in *Proc. of the 17th Int. Conf. on Digital Audio Effects (DAFX-15)*, 2015.

[12] E. Rank and G. Kubin, "A waveguide model for slapbass synthesis," in *IEEE Int. Conf. on Acoust., Speech, and Sig. Proc.*, 1997, vol. 1, pp. 443–446.

[13] L. Trautmann and R. Rabenstein, "Multirate simulations of string vibrations including nonlinear fret-string interactions using the functional transformation method," *Appl. Signal Proc.*, vol. 7, pp. 949–963, 2004.

[14] P. Kramer, J. Abeßer, C. Dittmar, and G. Schuller, "A digital waveguide model of the electric bass guitar including different playing techniques," in *Proc. Int. Conf. Acoust. Speech Sig. Proc.*, 2012, pp. 353–356.

[15] V. Chatziioannou and M. van Walstijn, "An energy conserving finite difference scheme for simulation of collisions," in *Sound and Music Computing (SMAC-SMC 2013)*, 2013.

[16] S. Bilbao, A. Torin, and V. Chatziioannou, "Numerical modeling of collisions in musical instruments," *Acta Acustica united with Acustica*, vol. 101, no. 1, pp. 155–173, 2015.

[17] V. Chatziioannou and M. van Walstijn, "Energy conserving schemes for the simulation of musical instrument contact dynamics," *J. Sound and Vibration*, vol. 339, pp. 262–279, 2015.

[18] S. Bilbao, "Numerical Modeling of String/Barrier Collisions," in *Proc. of the Int. Symp. Musical Acoustics (ISMA)*, 2014.

[19] M. van Walstijn and V. Chatziioannou, "Numerical simulation of tanpura string vibrations," in *Int. Symp. on Musical Acoustics (ISMA)*, 2014.

[20] J. Bridges and M. van Walstijn, "Investigation of tanpura string vibrations using a two-dimensional time-domain model incorporating coupling and bridge friction," in *Third Vienna Talk on Music Acoustics, At Vienna, Austria*, 2015, pp. 126–131.

[21] J. Woodhouse, "Plucked guitar transients: Comparison of measurements and synthesis," *Acta Acustica united with Acustica*, vol. 90, no. 5, pp. 945–965, 2004.

[22] C. Valette and C. Cuesta, *Mécanique de la corde vibrante*, Hermes, Paris, 1993.

[23] V. L. Popov, *Contact Mechanics and Friction: Physical Principles and Applications*, Springer, Heidelberg, New York, 2010.

[24] B. Bank, "Direct design of parallel second-order filters for instrument body modeling," in *Int. Comp. Music Conf. (ICMC)*, 2007, pp. 458–465.

[25] J.M. Adrien, "The missing link: Modal synthesis," in *Representations of Musical Signals*, Giovanni De Poli, Aldo Piccialli, and Curtis Roads, Eds., chapter 8, pp. 269–298. MIT Press, Cambridge, MA, USA, 1991.

[26] L. Trautmann and R. Rabenstein, *Digital Sound Synthesis by Physical Modelling Using the Functional Transformation Method*, Kluwer Academic / Plenum Publishers, 2003.

[27] F. Avanzini and R. Marogna, "A modular physically based approach to the sound synthesis of membrane percussion instruments," *IEEE Trans. Audio, Speech, and Lang. Proc.*, vol. 18, no. 4, pp. 891–902, 2010.

[28] M. van Walstijn and J. Bridges, "Simulation of distributed contact in string instruments: a modal expansion approach," in *Proc. Europ. Sig. Proc Conf (EUSIPCO2016)*, Accepted for publication, 2016.

[29] S. Bilbao, "Modal type synthesis techniques for nonlinear strings with an energy conservation property," in *Proc. Int. Conf. Digital Audio Effects (DAFx-04)*, 2004, pp. 119–124.

[30] S. Bilbao and J. O. Smith, "Energy-conserving finite difference schemes for nonlinear strings," *Acta Acustica u/w Acustica*, vol. 91, no. 2, pp. 299–311, 2005.

[31] S. Bilbao, A. Torin, P. Graham, J. Perry, and G. Delap, "Modular Physical Modeling Synthesis environments on GPU," in *Int. Comp. Music Conf. (ICMC)*, 2014, pp. 1396–1403.

[32] F. Pfeifle and R. Bader, "Real-time finite difference physical models of musical instruments on a field programmable gate array (FPGA)," in *Proc. Int. Conf. Digital Audio Effects (DAFx-12)*, 2012.